CMLS, Cell. Mol. Life Sci. 59 (2002) 2144–2154
1420-682X/02/122144-11

CMLS Cellular and Molecular Life Sciences

Research Article

Structural features of prions explored by sequence analysis. II. A PrP^{Sc} model

J.-P. Mornon *, K. Prat, F. Dupuis, N. Boisset and I. Callebaut

Systèmes Moléculaires & Biologie Structurale, LMCP, CNRS UMR 7590, Universités Paris 6 et Paris 7, case 115, 4 place Jussieu, 75252 Paris Cedex 05 (France), Fax + 33 1 44 27 37 85; e-mail: mornon@lmcp.jussieu.fr

Received 29 July 2002; received after revision 24 October 2002; accepted 24 October 2002

Abstract. Prion diseases are neurodegenerative disorders associated with a conformational conversion of the prion PrP protein, in which the β strand content increases and that of the α helix decreases. However, the structure of the pathogenous form PrP^{Sc}, occurring after conformational conversion of the normal cellular form PrP^{C}, is not yet known. From sequence analysis, we have previously proposed that helix H2 of the prion PrP^{C} structure might be a key region for this structural conversion. More recently, we identified the TATA box-binding protein fold as a putative scaffold that may locally satisfy the predicted secondary-structure organisation of PrP^{Sc}. In the present analysis, we detail the schematic construction of PrP^{Sc} monomeric and dimeric models, based on this hypothesis. These models are globally compatible with available data and therefore may provide further insights into the structurally and functionally elusive PrP protein. Some comments are also devoted to a comparison of the yeast Ure2p prion and animal prions.

Key words. Prion; Ure2p; cystatin; TATA box-binding protein; swapping; fusion peptide; HCA.

Animal prion proteins (PrPs) constitute a homogenous and 'closed' family at the level of their amino acid sequences, a feature which precludes an easy detection of structurally and functionally related proteins [1, 2]. The function(s) of the normal PrP^{C} protein, as well as the structural mechanisms leading to the conversion of the normal PrP^{C} form to the pathogenous PrP^{Sc} one, have remained largely elusive [3]. However, this conversion is known to be associated with a large increase in β strand content and a decrease in α helix content, and is a key feature of fibril formation. The comparison of monomeric [see e.g. refs 4–6] and dimeric [7] structures of globular domains of the normal PrP^{C} protein highlighted some regions that could be involved in the structural conversion. Noticeably, in the dimeric form, the C-terminal part of helix H2 is transformed into a β strand and helix H3 swaps from one monomer to the other. Some data to further understand the PrP protein were offered by other experimental structures, such as that of the PrP-related Doppel protein [8] and those of the distinct yeast prion Ure2p [9, 10]. Although not related at the sequence and three-dimensional (3D) levels, the yeast prion Ure2p shares with PrP a common overall architecture, made of repeated or pseudo-repeated sequences in the N terminus and with a C-terminal globular domain. Moreover, in Ure2p and PrP, segments of approximately 20 amino acids have been identified, which exhibit an unusual flexibility and may be a trigger factor of prion aggregation.

To tentatively gain new insights into this question, we used a battery of sequence analysis tools, especially hydrophobic cluster analysis (HCA) [11, 12] and suggested [13] that: (i) the foamy viruses have likely included in their envelope proteins a domain sharing clear similarities with human prion (from amino acid 95 to the end of the sequence) and with the entire Doppel protein, (ii) an

* Corresponding author.

interferon-inducible membrane protein shares sequence and putatively 3D similarities with prion and Doppel proteins (from amino acids 135 and 35, respectively, to the end of the proteins), (iii) the C-terminal half of the TATA box-binding protein (TBP) fold may locally constitute a template for the structure of the globular domain of the pathogenous PrP^{Sc} (in monomeric as well as in dimeric forms), occurring after 3D conversion of the non-pathogenous cellular form PrP^{C}.

In this paper, we focused on the construction of PrP^{Sc} models and showed that they may globally account for the recent data obtained for two-dimensional (2D) crystals of PrP variants [14].

Material and methods

Sequence analysis

Additional analyses of sequences were performed as described previously [13] and principally using the HCA approach [11, 12].

Modelling

Protein Data Bank (PDB) [15] entries and protein structures were manipulated using SwissPDBviewer [16, 17], with which illustrations were also made.

Results and discussion

PrP^{Sc} model units: construction of PrP^{Sc} models, based on the structures of human prion and the C-terminal half of the TBP fold

From sequence analysis [12, 13], we hypothesised that the second helix of the globular domain of PrP^{C} (helix H2; see fig. 1A) for a schematic representation of the PrP^{C} structure) and its immediate vicinity are converted in the PrP^{Sc} structure into three successive, likely antiparallel β strands (fig. 1A). The third strand (purple) of the converted helix H2 is thus expected to lie at the same sequence location as the strand observed in the crystalline swapped dimer of PrP^{C} [7], which does not exist in the nuclear magnetic resonance (NMR) monomeric form [4–6]. The C-terminal part of the PrP^{Sc} globular domain was therefore thought to consist of three strands followed by a stable helix (helix H3). Searching for a structural template possessing such a succession of secondary structures [13] highlighted the structure of a TBP [18] (fig.1B). The TBP dimer consists of a twisted β sheet made of ten antiparallel β strands, covered by four helices (a short one and a long C-terminal one, in each monomer). This sheet is very similar to that of the amyloidogenic dimeric transthyretin (TTR) protein [19] (data not shown). Introducing this local TBP template in the monomeric and dimeric structures of PrP^{C} led to plausible models in which a Cys179–Cys214 disulphide bridge can be formed (figs. 1C, 2). This disulphide bridge indeed exists in both the PrP^{C} and PrP^{Sc} structures. Hereafter, we detail this construction, considering the following features.

1) Monomeric prion (NMR structure) versus dimeric prion (X-ray structure) (fig. 2A). Two important, likely interdependent, features distinguish these conformers: (i) the presence of a new β strand (purple) replacing the C-terminal part of helix H2 and (ii) the swapping of the long terminal helix H3 between subunits (blue) [see ref. 20 for a review on swapping, which can be briefly described as the process in which one or several secondary-structure elements of a protein break their non-covalent bonds with the remainder of the molecule, the equivalent elements of a second identical molecule taking their place].

As commented previously [7, 13], the crystalline dimeric conformer of prions may constitute a link between the classical PrP^{C} monomeric form, repeatedly observed in NMR experiments, and the pathogenous PrP^{Sc} one that forms fibrils. This dimeric form lacks a higher β strand content, but additional rearrangements involving the C-terminal part of helix H2 and the following loop may provide a crucial step towards the high β strand content of PrP^{Sc}.

2) A proposal for the $\alpha \rightarrow \beta$ conversion, with helix H2 as a key region. As detailed previously [13], we propose that the putative full conversion of H2 and of its immediate neighbourhood into three successive β strands (S3, S4, S5) (fig. 1A) satisfies a prerequisite for the emergence of the PrP^{Sc} structure. This hypothesis is illustrated in figure 2B, C. Another hypothesis [14] favours the involvement of the solvent-exposed helix H1, while other results [21] further support the involvement of helix H2. Indeed, the simulations performed by Gilis and Rooman [21] indicate that helix H1 is intrinsically stable in contrast to helix H2. Noticeably, helix H1 is stabilised by four

Figure 1. Proposed conversion of the PrP^{C} helix H2 in three successive antiparallel strands, as expected for PrP^{Sc}. (*A*) Schematic representation of the mature PrP architecture. Secondary structures, as observed in NMR (1) and X-ray (2) experiments are coloured (red, strand S1; orange, helix H1; yellow, strand S2; green, helix H2; blue, C-terminal helix). The disulphide bridge is symbolised by a solid line. A third strand (purple, S3) appears in the crystalline swapped dimer, together with the swapping of helix H3. (3) represents the schematic conversion of helix H2, as proposed here, into three successive strands S3, S4 and S5, centred around positions 170, 178 and 190. (*B*) Comparison of the HCA transpositions of part of the sequences of human prion and of human TBP (domain 1), adapted from Mornon et al. [13]. Guidelines to the use of HCA can be found elsewhere [12, 13]. Briefly, the sequence is shown on a duplicated helical net, in which hydrophobic amino acids (V, I, L, M, F, Y, W) are contoured. These latter form clusters whose positions mainly match those of regular

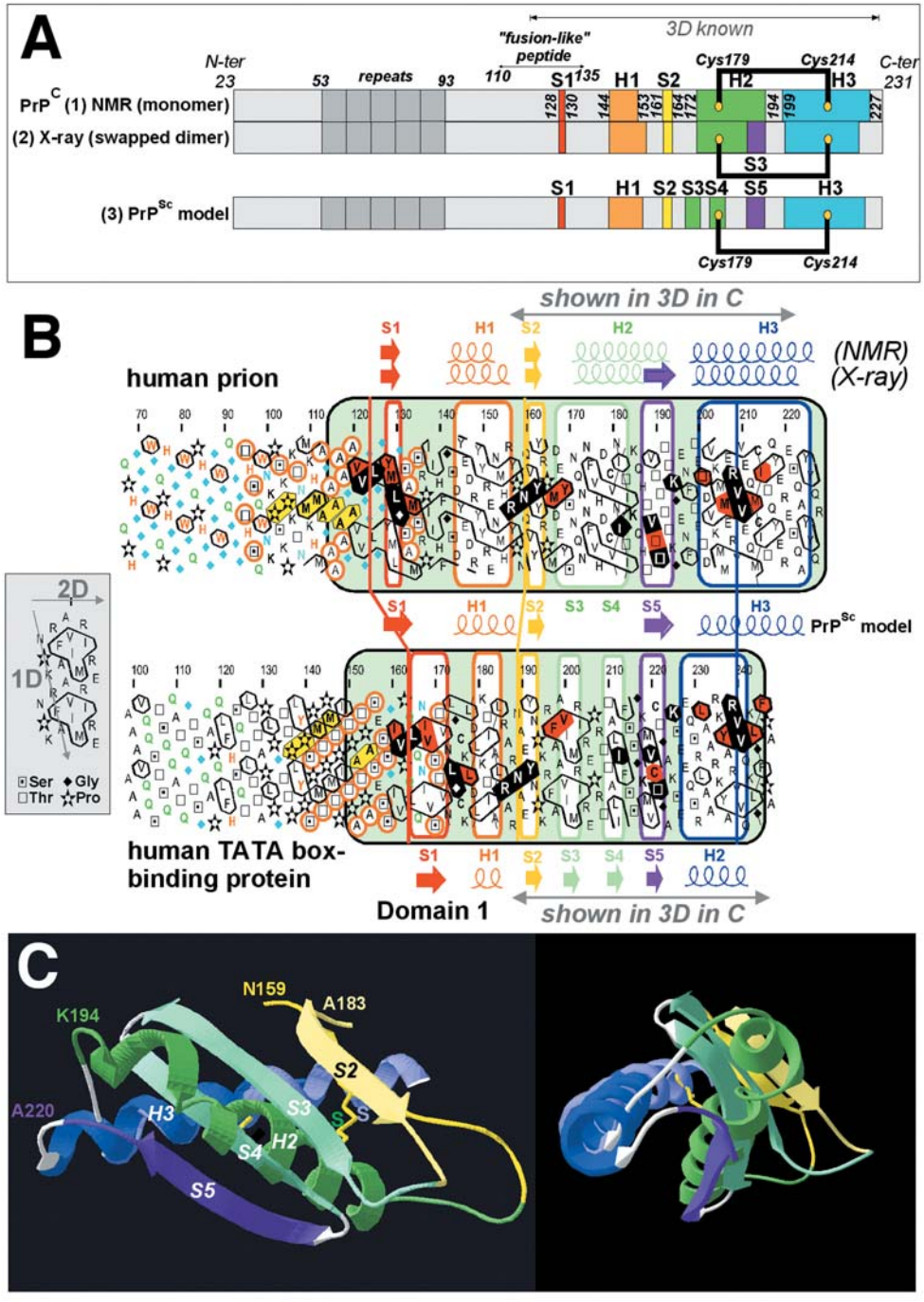

Figure 1 (continued)

secondary structures. The way to read the sequence as well as symbols used for four amino acids are indicated in the shaded inset. The observed secondary structures for the two proteins are indicated above and below the plots, respectively. The secondary structure expected for PrP^{Sc} (PrP^{Sc} model) is repeated between the two plots. (*C*) Two nearly orthogonal views of the N159–Q217 fragment of human monomeric PrP^{C} (PDB code 1qlx) and of the A183–K239 fragment of human TBP (PDB code 1cdw) (58 and 56 amino acids, respectively; two sequences shown by arrows in *B*), based on the superimposition of strands S2 and C-terminal helices (light blue, PrP^{C}; dark blue, TBP) and according to the alignment proposed by Mornon and colleagues [13] and partially shown in *B*. Fourteen amino acids are involved (PrP^{C} 161–163/203–213; TBP 186–188/230–240) and result in a 2.5-Å root mean square (rms) deviation for Cα [1.7 Å if a nearly colinear slipping of the C-terminal helices (light and dark blue) is taken into account]. These values are similar to the mean rms observed between the whole structures of human and mouse cores (1qlx and 1ag2, respectively; 2.5 Å). The green helix H2 of PrP^{C} is replaced in TBP by three successive antiparallel strands (S3, S4, S5) shown in light green and purple, respectively. The PrP^{C} C179–C214 disulphide bridge is shown in yellow between helices H2 (green) and H3 (light blue). In the centre of the left view, the position which will be occupied by C179 in the putative PrP^{Sc} structure is shown on strand S4 of TBP. This position is shifted by one amino acid with respect to the ideal alignment reported in *B* [13]. A nearly α helix two-turns coaxial 3D shift of helix H3, mainly preserving its global hydrophobic/hydrophilic balance with respect to its environment, then allows a new disulphide bridge between Cys179 and Cys214.

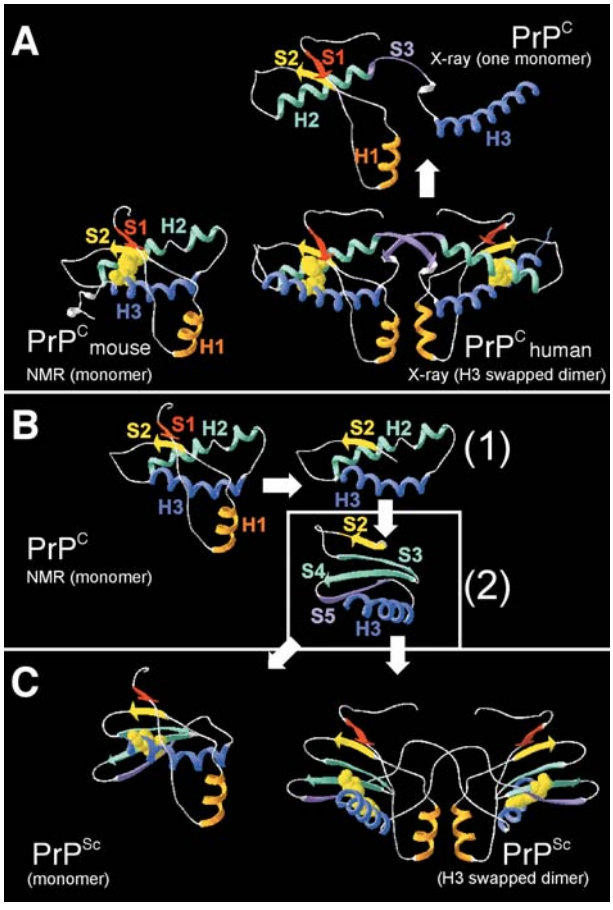

Figure 2. From the PrP^C globular domain structure to a model of PrP^{Sc}, locally based on the TBP structure. (*A*) Ribbon representation of the PrP^C structure in the observed monomeric (mouse PrP^C NMR; PDB identifier 1ag2) and swapped dimeric (human PrP^C X-ray; PDB identifier 1i4m) conformers. For clarity, one monomer of the dimeric form has been isolated at the top. Secondary structures are coloured as in fig.1 A, according to Mornon et al. [13]. Yellow spheres indicate the disulphide bridge. Note that the C terminus of helix H3 is differently accommodated from one PrP^C to the next, after position 216, i.e. after the disulphide bond linking Cys179 and Cys214. (*B*) Focus on the C-terminal region [yellow strand S2 to blue helix H3, panel 1; and conversion of helix H2 (green) into three successive β strands (green and purple, inset 2], as found in part of the 3 D structure of human TBP (PDB identifier 1cdw), coloured in a similar way. (*C*) Construction of putative monomeric and dimeric models of the PrP^{Sc} globular domain, as a concatenation of the templates of PrP^C (*A*) and TBP (*B*, panel 2). A Cys179–Cys214 disulphide bridge is retrieved between the second strand of the sheet, substituting helix H2 (green) and the unmodified helix H3 (blue). Within the hypothetical PrP^{Sc} swapped dimeric model, each monomer would share with its neighbour a similar interface as in the X-ray PrP^C form, as built by helix H1 (orange) and long extended segments of sequence. Connection between the swapped helix H3 and the monomeric PrP^{Sc} core of the same polypeptidic chain is assumed to be partly ensured through a limited unwinding of the N terminus of this helix (unwinding/winding of ends of helices is common in protein structures as these depend only on the considered local segment of sequence).

side chain i→i + 4 interactions on a 9-amino acid interval (polar D144–R148, R148–E152, D147–R151, aromatic Y145–Y149). We have proposed from sequence data [13] that the central part of the C-terminal helix H3 (~204–216) stays invariant through conversion, a hypothesis which is thus in agreement with its high stability in PrP^c [22]. The present analysis is further supported by the recent study of Dima and Thirumalai [23], who also clearly identified helix H2 as particularly frustrated in its α state in the monomeric mammalian PrP^c structure and by that of Karlberg and colleagues [24] who made similar observations. Very recently, Kuwata and colleagues [25] also showed the likely existence of a PrP* intermediate conformer in which helices H2 and H3 are preferentially disordered.

3) Involvement of the region encompassing amino acids 90–120 in $PrP^c \rightarrow PrP^{Sc}$ conversion. Some data have been proposed to support the participation of this segment in the conformational change [26, 27]. In agreement with this hypothesis, we note that it includes part of a 'fusion-like' peptide [28] that we propose to be the driving force of, or at least to be associated with the overall conversion of the prion protein, as already observed in other proteins possessing such peptides [13]. On the other hand, the likely mobile β strand S1 (YML; amino acids 128–130, red) within the fusion-like peptide is in contact with β strand S2 (VYY; amino acids 160–162, yellow), which we propose here to be associated with a newly formed β strand (S3, green), rich in asparagine and glutamine, at the N terminus of helix H2. This β strand S3 may extend between Asp167 and Asn174, and has been putatively more precisely localised on the basis of the alignment of its sequence with the IVV pattern (amino acids 154–156) of the human foamy virus envelope [13]. We assume that helix H1 stays helical, although its isolated state may favour some structural conversion. Moreover, its position likely moves more or less with respect to its neighbours during the conformational change.

4) Schematic construction of PrP^{Sc} globular cores. According to the TBP template, which may account for the $\alpha \rightarrow \beta$ conversion of helix H2, and on the basis of the monomeric and dimeric swapped X-ray structures of PrP^c, we constructed new cores, substituting the S2-H2 (monomer, yellow and green) or the S2-H2-S3 (swapped dimer, yellow, green and purple) secondary-structure sets of the PrP^c structures, shown in figure 2 A, by strands S2-S3-S4-S5, as they are observed in the TBP structure (in yellow, green and purple in fig. 2 B inset 2 and in fig. 1). The 3D superimposition of strand S2 and helix H3 of PrP on strand S2 and helix H2 of TBP, according to the HCA sequence alignment (fig. 1), results in a good match of ~2-Å rms on Cα. Between them, the PrP H2 is replaced

by three strands in TBP (S3, S4, S5). As detailed previously [13], only a few insertions and deletions are needed and the amino acid substitutions of the TBP template by prion residues did not lead to significant difficulties nor to non-relaxable steric hindrances. The long C-terminal helix H3 of PrP^{c} (blue) and the equivalent one of the TBP remain colinearly superimposed during this construction (fig. 1). Thus, the PrP^{Sc} models are obtained by the 3D superimposition/concatenation of PrP^{c} S1-H1-S2-H3 elements with the S2-S3-S4-S5-C-terminal helix of TBP (fig. 1). These substitutions resulted in overall coherent models of what might be the monomeric and swapped dimeric globular units of PrP^{Sc} (fig. 2C), which resemble the globular PrP^{c} structure. These preliminary models thus appeared to be suitable for further refinements. Importantly, the concatenation of the PrP^{C} and TBP templates allowed a disulphide bridge between Cys179 in strand S4 (located in the PrP^{C} structure in helix H2) and Cys214 in helix H3. Indeed, the PrP protein in the PrP^{Sc} form keeps a disulphide bridge in this position, which is likely an intra-molecular one [see e.g. ref. 29], although the role of inter-molecular disulphide bridges has been questioned [30]. This newly formed S1-S2-S3-S4-S5 sheet appears to be complementarily stabilised through a putative Arg164-Glu168 salt bridge and a concentration of asparagine and glutamine side chains within strand S2 (Asn159, Gln160), strand S3 (Asn171, Gln172, Asn173, Asn174) and possibly helix H3 (Gln217), a cluster in which a complex H-bond network may occur. Otherwise, the overall similarity between PrP^{C} and PrP^{Sc} is in favour of the emergence of mixed PrP^{C}/PrP^{Sc} structures, like heterodimers (fig. 3C) that have been proposed to exist during prion replication [31–33, debated in ref. 34]. This dimeric PrP^{Sc} model allowing PrP^{C}/PrP^{Sc} heterodimers is also in accordance with the identification of the 95–170 segment as the binding site of PrP^{C} to PrP^{Sc} [1].

Figure 3A, B illustrates some features of the hypothetical swapped dimeric model of PrP^{Sc}, compared to the PrP^{C} crystallographic dimer. Of interest is the clustering of important prion mutations at the dimer interface, as well as in the region proposed to be crucial for the conversion of helix H2 into three successive β strands. Figure 4 shows that the conversion of the monomeric PrP^{C} unit, based on the TBP template, leads to a PrP^{Sc} model that possesses some common 3D features with monomers of the amyloidogenic cystatin protein family [35, 36]. The two folds are similarly built around a five-stranded antiparallel β sheet covered by a long helix. However, the two polypeptides run in opposite directions, the long helix covering the β sheet being C terminal in the prion and N terminal

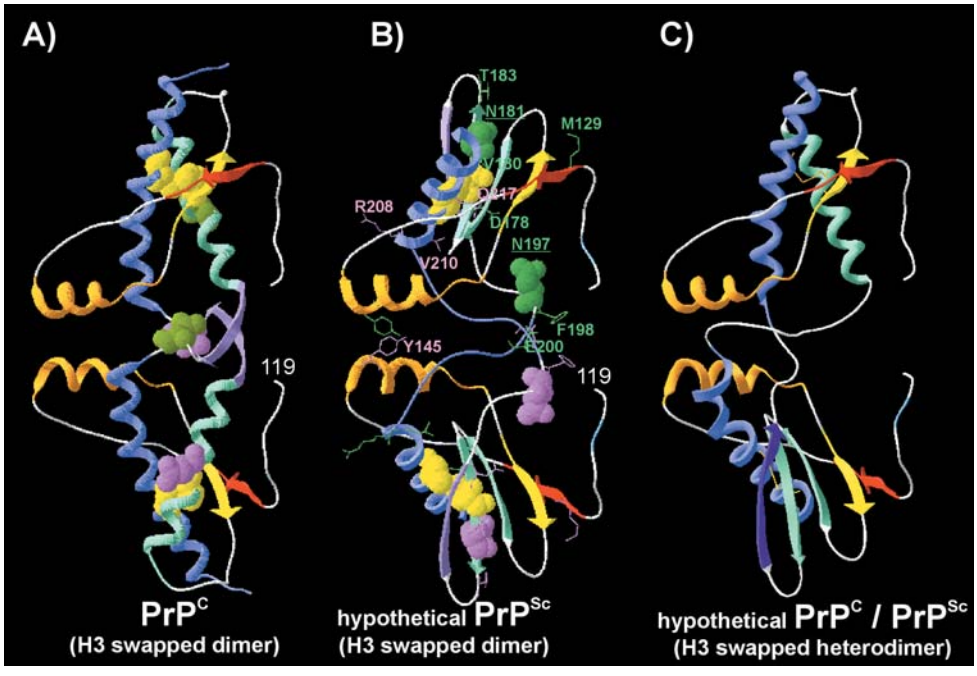

Figure 3. Comparison of the observed PrP^{C} (*A*) and hypothetical PrP^{Sc} (*B*) swapped dimers. Both chains are similarly coloured. Cys179 and Cys214, forming a disulphide bridge, are depicted as yellow balls, whereas Asn181 and Asn197, linking sugars, are shown as pink or green balls respectively, in each monomer. Within the PrP^{Sc} model, the short N-terminal light-blue chains indicate a putative short β strand, centred on Val121 and Val122, which may join the strand S1 (red) within the main β sheet. Important mutations of the prion sequence are indicated in *B*. They appear to cluster in the dimer interface and in the region involved in H2 conversion. (*C*) Schematic modelling of a PrP^{C}/PrP^{Sc} swapped heterodimer. The main PrP^{C} and PrP^{Sc} cores are at the top and bottom, respectively. The disulphide bridges are indicated in both cores. With respect to the PrP^{Sc} homodimer (*B*), the heterodimer likely implies a partial winding of the N-terminal part of helix H3.

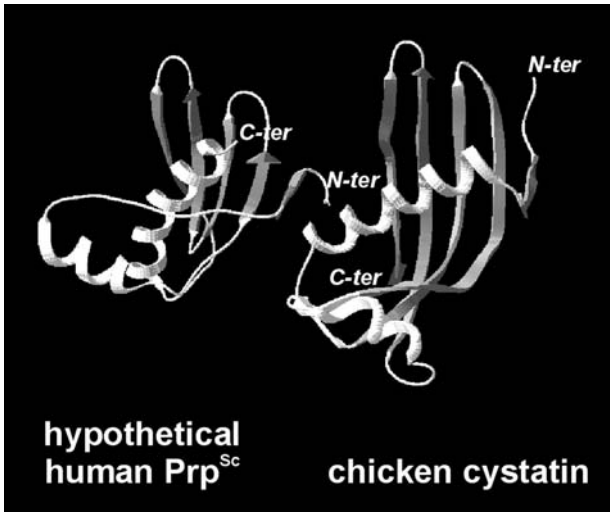

Figure 4. Comparison of the monomeric PrP^{Sc} model proposed in the present study with the amyloidogenic protein cystatin monomer (see text). Cystatin PDB code is 1cew.

in cystatin. Cystatin likely forms fibrils after dimerisation and swapping of one strand and of the adjacent long helix [35, 36].

PrP^{Sc} model units: the model of the PrP^{Sc} swapped dimer fits some main features derived from electron crystallography

A recent electron crystallography study of N-terminally truncated PrP^{Sc} 27–30 (amino acids 89–end) and of PrP^{Sc} 106 'miniprion' (amino acids 89–140 + 176–end) showed isomorphous 2D crystals, coexisting along side prion rods and possessing a likely trigonal (pseudo-hexagonal) symmetry with a unit cell of a = b = 69 Å [14]. Figure 5A shows that the assembly of three PrP^{Sc} dimer models, constructed as detailed above, nicely fits the space around a three-fold axis, giving rise to a pseudo-hexagonal structure. The size of this structure is in agreement with the observed cell taking into account space that would be occupied, outside the assembly described above, by large sugars (which likely expand outside the

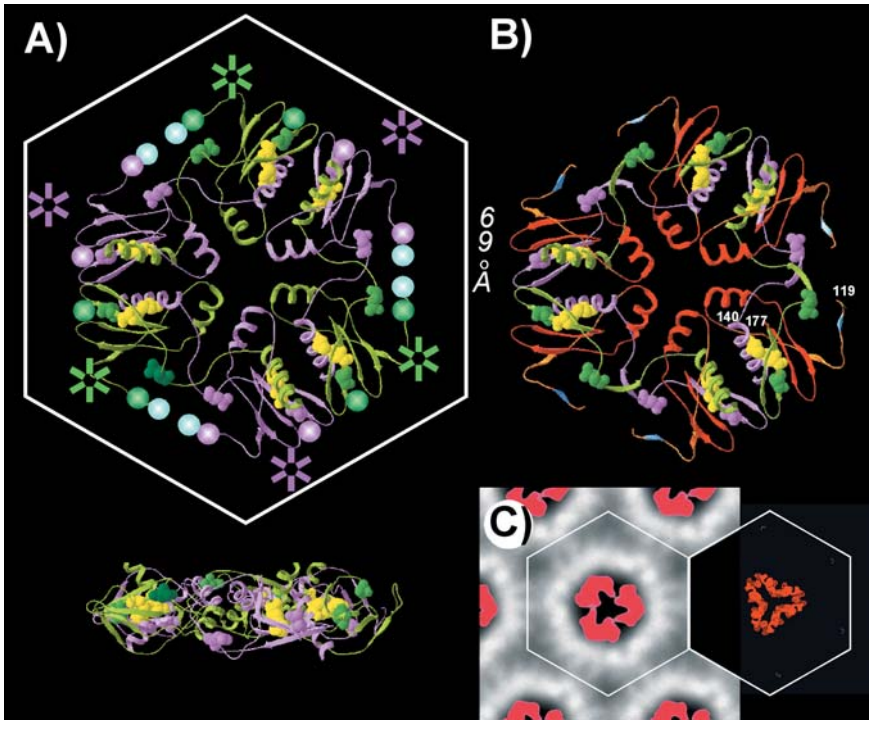

Figure 5. Assembly of dimeric PrP^{Sc} models. (*A*) Putative trimer of dimers in two orthogonal views. Within each dimer, one monomer is coloured pink, the other green. Disulphide bridges are shown with yellow balls and asparagine sugar linkers with pink or green van der Waals rendering. Large pink and green balls symbolise the sugars themselves and blue ones the 90–118 missing segments, the modelling of which is out of the scope of the present study and whose exact location is unknown. However, the nearly six-fold distribution of sugars shown in this figure is in good qualitative agreement with their experimental localisation, recalled here by coloured stars, which symbolise the likely centres of sugar densities (cf. fig. 3F of the work of Wille and colleagues [14]). The size of the 2D crystal unit cell of PrP^{Sc} (Prp27–30) [14] is indicated in white to the right. (*B*) Same as *A*, with the 141–176 peptide coloured red; a putative additional β strand centred on Val121-Val122 is shown in light blue. (*C*) At left, a reproduction of the PrP^{Sc} 106 minus PrP^{Sc} 27–30 statistically significant substraction map published by Wille and colleagues [fig. 3E in ref. 14], which mainly maps the location of the large acidic clusters within the 141–176 deletion existing between PrP^{Sc} 27–30 and PrP^{Sc} 106 as the consequence of the difference of UO_2^+ staining between the two PrP species. A van der Waals rendering of D144, E146, D147, E152 within helices H1 at the centre of the present assembly is shown at right and matches well the expected data.

mean plane of the trimers) and by the non-modelled structure of the segment ranging from amino acids 90 to 118. These features are in good agreement with conclusions derived by Wille and colleagues [14] from the crystals: indeed, the favoured hypothesis is the assembly of trimers of dimers, with residues 143–177 (in which H1 is situated) in the centre of the cell and nanogold-labelled sugars in the periphery. The Δ 141–176 deletion, leading to the '106' mini-prion, is coloured red in figure 5B and illustrates the consequence of removing these 36 amino acids in this model. Amino acids 140 and 177 are not far from each other (13.8 Å) and in direct view. Therefore, they may be linked together after a limited structural reorganisation. Meanwhile, the N-terminal part (from amino acids 119 to 140) may move and replace strands S2 and S3 by strand S1 and a preceding putative strand centred on Val121 and Val122, shown in blue in figure 5B. In this way, the outside ring of the trimer may be preserved, linking subunits and thereby possibly accounting for the isomorphism observed between PrP^{Sc} 27–30 and PrP^{Sc} 106 crystals. Moreover, one should note that in the swapped PrP^{C} dimer, positions 140 and 177 are more separated (e.g. 18.5 Å in human PrP^{C} and 20.3 Å in mouse PrP^{C}) than in the present PrP^{Sc} model and, perhaps more importantly, are hidden from each other by helix H3, suggesting that such a hypothetical PrP^{C} 106 would not be stable without large structural modifications. However, the similar overall shapes of PrP^{C} and the PrP^{Sc} model may authorise mixed PrP^{C}-PrP^{Sc} in such 2D crystalline assemblies.

The trimeric assembly of PrP^{Sc} dimers shown in figure 5A clusters Asp and Glu amino acids, and noticeably six times in its centre D144, E146, D147, E152, E207 and E211. This feature is in good agreement with expectations from the electron crystallography observations, i.e. a concentration of negative charges in complex with uranyl ions, leading to dark areas in the centre of the 2D crystal [14]. Moreover, the statistically significant PrP^{Sc} 106 minus PrP^{Sc} 27–30 substraction map published by Wille and colleagues [14] (fig. 5C), which does mainly map the location of the large acidic cluster within the 141–176 deletion between PrP^{Sc} 27–30 and PrP^{Sc} 106 (i.e. the difference behaviour of uranyl acetate staining between the two crystals), matches well the location proposed here of D144, E146, D147 and E152 (fig. 5C). Two other acidic amino acids (D167, E168) are present in the 141–176 segment. In our model, they are at the periphery of the shown assembly and roughly correspond to a second but faint density in the substraction map [fig. 3C in ref. 14; data not shown].

An alternative arrangement of dimeric PrP^{Sc} models has been considered, with helices H1 pointing outside towards corners of the cell and not, as in figure 5A, towards its centre. The resulting packing, although sterically plausible, places the sugar links and the N-ter parts towards the centre, and thus fails to match as the packing suggested by the substraction maps between the isomorphous crystals of PrP^{Sc} 27–30 and PrP^{Sc} 106.

Alternatively, non-swapped PrP^{Sc} monomers may also replace H3 swapped dimers in these crystals.

The proposed models of PrP^{Sc} monomer and dimer, which fit published data, may therefore add new data to previous modelling studies [37, 38] and to the recently published models that have been designed to accord with the main observed features of the reported 2D crystals [14]. These latter models are based on the hypothesis of the invariance of helices H2 and H3 [39], and of the disulphide bridge linking them with respect to their positions in the PrP^{C} monomer. In this study, the preceding segment (amino acids ~89 to 175) is assumed to adopt a regular β helix conformation. This β structure is not completely at variance with the sequence composition of this segment, in which amino acids such as Gly, Asn or Ala, as well as Tyr may favour its emergence. However, no recurrent folding motif that may clearly favour β helices can be observed regularly distributed along this segment, a situation also pertaining to TTR [40]. Assuming the existence of this β helix, this model easily accounts for the 141–176 deletion, but with more difficulties for putative swapping [39]. We suggest that the driving force of this proposed β helix conversion, if it really occurs in this way, may also be the 'fusion-like' peptide, which is included in this 90–175 segment. However, at present, speculating further on these data is difficult, and particularly on what should happen to the prion structure when a large deletion such as 141–176 occurs.

In conclusion, the models of PrP^{Sc} monomer and dimer proposed here and derived from sequence analysis, limited to the prion globular domains [they lack repeats and the immediate downstream segment (amino acids 90–118)], exhibit the following important structural features:

1) The conversion of the PrP^{C} helix H2 on the template of the TBP fold from its α state to three successive antiparallel β strands allows a disulphide link between Cys179 (in strand S4) and Cys214 (in helix H3), expected to be conserved in PrP^{Sc}, and significantly increases the β strand content of PrP, which may be further extended by PrP^{Sc} aggregation, noticeably in the vicinity of strand S1 within the fusion-like peptide.
2) The structures of PrP^{C} and PrP^{Sc} easily suggest heterodimers, the existence of which is thought to be important to trigger the conversion between the two PrP forms.
3) The positions of amino acids 140 and 177 within the PrP^{Sc} model are compatible with the existence of the PrP 106 mini-prion obtained after deletion of the 141–176 segment, as they are not far and are in direct view of each other.

4) The PrP^{Sc} dimer model fits well the experimental observation made on PrP^{Sc} 27–30 and PrP^{Sc} 106 2D crystals and is therefore further supported by these data. A very recent study of several PrP peptides by Jamin and colleagues [41] is also in good accordance with our basic hypothesis, in particular concerning helices H1 and H2.

Yeast Ure2p prion shares some overall structural features with animal prions and also exhibits secondary structure-frustrated sequence segments in its 3D structure

Let us compare some basic structural features of yeast Ure2p and human PrP prions, although these two proteins are clearly distinct and unrelated.

The crystal structure of the yeast Ure2p prion protein [9, 10, 42] has brought interesting data to further investigate a putative common structural behaviour of prion proteins.

Figure 6 compares the general 'texture' of yeast Ure2p and human prion sequences, a priori considered independent from each other. N-terminal regions of both proteins are characterised by different repeats, which are rich in asparagine, glycine and aromatic residues. The first part of a large central glutathione S-transferase-like dimerisable core, the counterpart of which is not present in human prion, is specific to yeast Ure2p. C-terminal to this region, a segment rich in alanine and threonine, specific to Ure2p, constitutes a flexible cap region, centred on the 'α cap' helix [9, 10, 43]. The C-terminal extremity of the first part of this GST-like dimerisable core (C-terminal part of helix α6) and the 'α cap' segment occupy within the Ure2p primary structure a position similar to that of the 'fusion-like' peptide/helix H1 segment of human prion, ending at the 'central proline' of PrP [13] (fig. 6). Some local sequence similarities [MAXA(5X)AXV(2X)L, X being any amino acid] are present in this region between the two proteins, as is a concentration of small amino acids (alanine, glycine, threonine). Downstream, the prion globular C-terminal domains share an overall common texture with local similarities centred on the 'central proline', and the two subsequent helices, which in Ure2p constitute the second part of the GST-like core. The shapes and amino acid composition of Ure2p hydrophobic clusters around positions ~270 (LVMEL), ~300 (VWLV) and ~325 (IGINIKIEF) are often found in

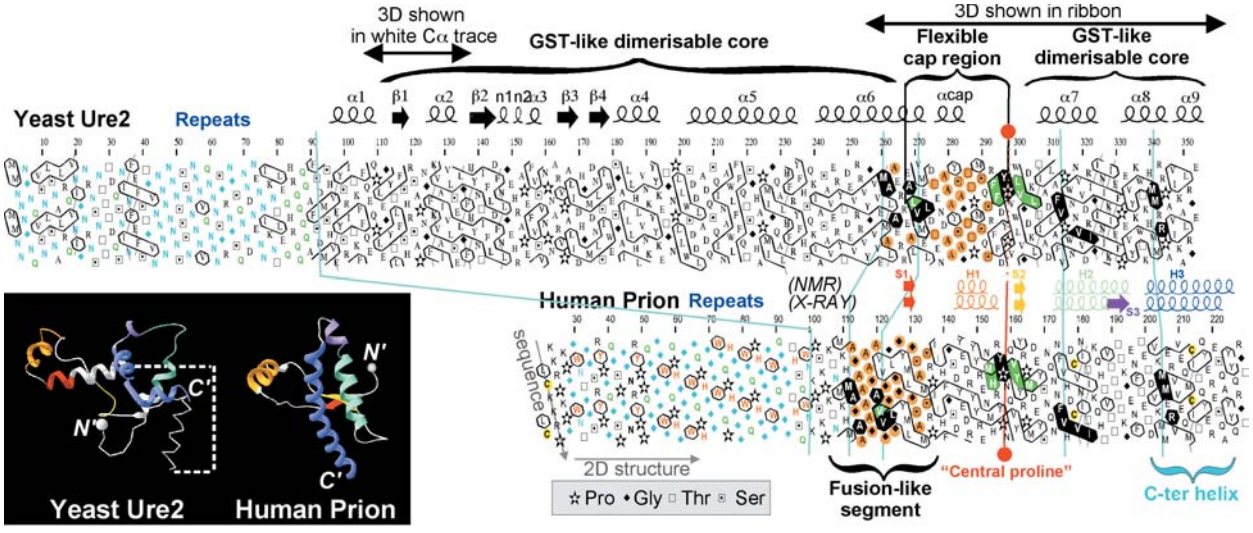

Figure 6. Sequence texture comparison of yeast Ure2p and human prions through HCA plots. The SwissProt accession numbers of human prion and yeast Ure2p are P04156 and P23202, respectively. Secondary structures, deduced from the experimental coordinates, are reported above the HCA plots [PDB identifier of yeast Ure2p: 1g6y; of human prion: 1qlx (NMR monomeric form) and 1i4m (X-ray dimeric form)]. Yeast Ure2p and human prion are similarly built with a non-globular N-terminal domain rich in repeated sequences and a mainly α C-terminal globular domain. Human prion contains in the N-terminal end of its globular domain a 'fusion-like' peptide and a highly hydrophilic helix H1, which could be tentatively compared to the extremity of helix α6 and the flexible α cap region of yeast Ure2p. The first part of a GST-like domain is present upstream of the α cap in Ure2p, which in the known crystal form constitutes the dimeric interface between two monomers. Sequence similarities (which do not imply that the two proteins are derived from a common ancestor, but might just suggest a potential local structural relationship) are shown with white letters on a black or green background and result in ~17% sequence identity over ~90 amino acids. At left, the 3D structures of the C-terminal domain of yeast Ure2p (PDB code 1g6y) and that of the monomeric form of human prion (PDB code 1qlx) are shown. The polypeptidic chains are coloured similarly as suggested by the comparison of sequence texture. Of interest are (i) the similar overall shape of the green-purple-blue segment, (ii) the proximity of the yellow and red ones, (iii) the similar position of the orange helices (Ure2p α cap and human prion helix H1), (iv) the location, relative to the represented cores, of the presently known N-terminal sequence atomic positions (N′, depicted as white balls) of yeast Ure2p (Q109) and of human prion [G119 (X-ray), G124 (NMR)], which attach the globular domains to the repeat-rich N-terminal domains. The white dotted line symbolises the central GST-like domain (from β2 to α6).

β strands while they actually correspond within the known 3D structure to α (first cluster) and coil (the two other clusters) regions. This is reminiscent of the situation we have discussed above for the helix H2 region of PrP. Noticeably, Ure2p α7 (amino acids 308–317; the putative 'counterpart' of PrP^{C} H2) is surrounded by α2 and the buried α5 helices, which both exhibit hydrophobic clusters typical of β strands [~amino acids 125 (FKVAIVL), 210 (INAWLFF), 230 (LHFRYF)]. However, this feature is expected for buried helices. Putatively, one or a few of these Ure2p segments might be involved in a limited and local structural conversion associated with the formation of certain fibrils [44]. The comparison between the experimental 3D structures of human prion and yeast Ure2p suggests further similarities between PrP and Ure2p, as illustrated in figure 6 in which the polypeptidic chain of Ure2p has been coloured according to the putative architectural correspondence established after comparison of its sequence texture with that of human prion. However, the significance of such a similar rough architecture of the C-terminal parts of PrP and Ure2p, if it is confirmed to be not fortuitous, needs new developments to be further understood.

Additional considerations

1) Prion and DNA. Prions have DNA strand transfer properties [45, 46]. As TBP interacts with DNA, one could speculate that the model of PrP^{Sc} proposed here, based on a hybrid structure between the TBP and the PrP^{C} one, may transitorily bind on its partly hydrophobic 'free' side small oligonucleotides, which can thus act as catalysts of conversion as well as assembling processes, as recently suggested [47, 48].

2) Driving force of the $PrP^{C} \rightarrow PrP^{Sc}$ conversion. The events that lead to this conversion remain largely unknown. Here, like some other groups [49–54], we have discussed further the possible role played by the prion 'fusion-like' peptide we have previously identified [28], which is specific to this protein and is not found in the paralogous Doppel sequence. The activity of fusion peptides and Serpin reactive centre loops, whose overall amino acid composition is similar to that of the 'fusion-like' peptide of prion, is made possible when one of their extremities is freed, liberated by proteolytic cleavage. So, an enzymatic cleavage of the prion protein, as is observed in a C-terminal fragment of PrP^{C} abundant in human brain [55], may allow the activation of the 'fusion-like' peptide which should be a crucial step in $PrP^{C} \rightarrow PrP^{Sc}$ conversion. Alternatively, the non-globular character of the PrP N-terminal part, upstream of the 'fusion-like' peptide, can confer enough freedom on its N-terminal end. We also proposed that the fusion-like peptide constitutes within PrP the first candidate, ouside the GPI anchor, to bind membranes, a feature suspected to interfere with the $PrP^{C} \rightarrow PrP^{Sc}$ conversion [see ref. 51 and references therein].

Met129 and Asp178 are key positions, of animal PrP proteins, because their related polymorphisms/mutations (Met→Val and Asp→Asn, respectively) lead to major pathological phenotypes [Online Mendelian Inheritance in Man (OMIM) 176640, and references therein]. Asp178 is the immediate neighbour of Cys179, which is implicated in the disulphide bridge. In the PrP^{C} structure, Met 129 (strand S1), Tyr162 (strand S2) and the Cys179 (helix H2)-Cys214 (helix H3) disulphide bridge are remarkably nearly colinear and separated by 3.1–3.4 Å from each other, while Asp178 points outside the protein core but establishes through its side chain a strong hydrogen bond with the side chain of Tyr128 [56], reinforcing, thereby, at long sequential distance the cohesion of this region. In our PrP^{Sc} model, Met129 (S1)-Tyr162 (S2)-Ser170 (S3) and the Cys179 (S4)-Cys214 (H3) disulphide bridge remain nearly colinear while Asp178 points towards Gln172 within a cluster of asparagine and glutamine residues belonging to strands S2 and S3, which also includes the mutated PrP Gln217 (H3). The Asp178Asn mutation would thus add an additional asparagine to this asparagine-glutamine cluster. In this context, we would stress the fact that Met129 (S1) belongs to the 'fusion-like' peptide and that Asp178 (PrP^{C} H2) is in the centre of strand S4 of the present PrP^{Sc} model. Consequently, it is tempting to speculate that one of the trigger factors in the $PrP^{C} \rightarrow PrP^{Sc}$ conversion may be the Met129-Asp178-Cys179 'hot' region of the PrP^{C} structure, the destabilisation of which may lead to the $\alpha \rightarrow \beta$ conversion.

3) Towards PrP^{Sc} aggregation and protofilament formation. In the TBP template, one face of the β sheet binds DNA. Therefore, the corresponding β sheet face in the TBP-derived PrP^{Sc} model (partially hydrophobic) remains 'free' to bind a new partner, which may be another PrP^{Sc} monomer.

This basic feature may suggest the association face to face of PrP^{Sc} monomers in a cross-β-like assembling, i.e. two infinite β sheets running in a helical way around each other with strands perpendicular to the axis of aggregation [40, 57], in which H3 swapping may also be present. Swapping is indeed a widespread and efficient means for assembling identical protein cores. Its potential role in PrP through helix H3 may therefore support the persistence of the central segment of this structure in PrP^{Sc} as proposed in the present hypothesis. Then, the structure of the PrP^{Sc} model leads to a peripheral location of the highly hydrophilic helix H1 and of its long connecting loops, as well as of the likely mobile C-terminal part of helix H3 and of sugars. Such a context that may occur in early steps of PrP^{Sc} 27–30 aggregation also appears favourable to the binding of repeats in the full PrP (which

possibly adopt a polyproline-II-like conformation [58]) all along a nascent protofilament and accounts well for the diameter of Scrapie-associated filaments (~50 Å) [59–61]. These features will be presented elsewhere.

Acknowledgments. The authors thank J. Doucet (LURE, Orsay, France) and A. Soyer (LMCP) for fruitful discussions and critical reading of the manuscript and H. Wille (UCSF, San Francisco, Calif.) for kindly providing us with a copy of a figure [14]. (Copyright 2002 National Academy of Sciences, USA).

1 Prusiner S. B. (1998) Prions. Proc. Natl. Acad. Sci. USA **95:** 13363–13383
2 Wopfner F., Weidenhöfer G., Schneider R., Von Brunn A., Gilch S., Schwarz T. F. et al. (1999) Analysis of 27 mammalian and 9 avian PrPs reveals high conservation of flexible regions of the prion protein. J. Mol. Biol. **289:** 1163–1178
3 Westaway D. and Carlson G. A. (2002) Mammalian prion proteins: enigma, variation and vaccination. Trends Biochem. Sci. **27:** 301–307
4 Riek R., Hornemann S., Wider G., Billeter M., Glockshuber R. and Wüthrich K. (1996) NMR structure of the mouse prion protein domain PrP (121–321). Nature **382:** 180–182
5 Riek R., Hornemann S., Wider G., Glockshuber R. and Wüthrich K. (1997) NMR characterization of the full-length recombinant murine prion protein, mPrP (23–231). FEBS Lett. **413:** 282–288
6 Zahn R., Liu A., Luhrs T., Riek R., Schroetter C. von, Lopez Garcia F. et al. (2000) NMR solution structure of the human prion protein. Proc. Natl. Acad. Sci. USA **97:** 145–150
7 Knaus K. J., Morillas M., Swietnicki W., Malone M., Surewicz W. K. and Yee V. C. (2001) Crystal structure of the human prion protein reveals a mechanism for oligomerization. Nat. Struct. Biol. **8:** 770–774
8 Mo H., Moore R. C., Cohen F. E., Westaway D., Prusiner S. B., Wright P. E. et al. (2001) Two different neurodegenerative diseases caused by proteins with similar structures. Proc. Natl. Acad. Sci. USA **98:** 2352–2357
9 Bousset L., Belrhali H., Janin J., Melki R. and Morera S. (2001) Structure of the globular region of the prion protein Ure2 from the yeast *Saccharomyces cerevisiae*. Structure **9:** 39–46
10 Umland T. C., Taylor K. L., Rhee S., Wickner R. B. and Davies D. R. (2001) The crystal structure of the nitrogen regulation fragment of the yeast prion protein Ure2p. Proc. Natl. Acad. Sci. USA **98:** 1459–1464
11 Gaboriaud C., Bissery V., Benchetrit T. and Mornon J. P. (1987) Hydrophobic cluster analysis: an efficient new way to compare and analyse amino acid sequences. FEBS Lett. **224:** 149–155
12 Callebaut I., Labesse G., Durand P., Poupon A., Canard L., Chomilier J. et al. (1997) Deciphering protein sequence information through hydrophobic cluster analysis (HCA): current status and perspectives. Cell. Mol. Life Sci. **53:** 621–645
13 Mornon J., Prat K., Dupuis F. and Callebaut I. (2002) Structural features of prions explored by sequence analysis. I. Sequence data. Cell. Mol. Life Sci. **59:** 1366–1376
14 Wille H., Michelitsch M. D., Guenebaut V., Supattapone S., Serban A., Cohen F. E. et al. (2002) Structural studies of the scrapie prion protein by electron crystallography. Proc. Natl. Acad. Sci. USA **99:** 3563–3568
15 Berman H. M., Westbrook J., Feng Z., Gilliland G., Bhat T. N., Weissig H. et al. (2000) The Protein Data Bank. Nucleic Acids Res. **28:** 235–242
16 Guex N. and Peitsch M. C. (1997) SWISS-MODEL and the Swiss-PdbViewer: an environment for comparative protein modeling. Electrophoresis **18:** 2714–2723
17 Kaplan W. and Littlejohn T. G. (2001) Swiss-PDB Viewer (Deep View). Brief Bioinform. **2:** 195–197
18 Nikolov D. B., Chen H., Halay E. D., Hoffman A., Roeder R. G. and Burley S. K. (1996) Crystal structure of a human TATA box-binding protein/TATA element complex. Proc. Natl. Acad. Sci. USA **93:** 4862–4867
19 Blake C. C. F., Geisow M. J., Oatley S. J., Rérat B. and Rérat C. (1978) Structure of prealbumin: secondary, tertiary and quaternary interactions determined by Fourier refinement at 1.8 Å. J. Mol. Biol. **121:** 339–356
20 Liu S. and Eisenberg D. (2002) 3D domain swapping: as domains continue to swap. Protein Sci. **11:** 1285–1299
21 Gilis D. and Rooman M. (2000) PoPMuSiC, an algorithm for predicting protein mutant stability changes: application to prion proteins. Protein Eng. **13:** 849–856
22 Hosszu L. L. P., Baxter N. J., Jackson G. S., Power A., Clarke A. R., Waltho J. P. et al. (1999) Structural mobility of the human prion protein probed by backbone hydrogen exchange. Nat. Struct. Biol. **6:** 740–743
23 Dima R. I. and Thirumalai D. (2002) Exploring the propensities of helices in PrP^{C} to form β sheet using NMR structures and sequence alignments. Biophys. J. **83:** 1268–1280
24 Karlberg Y., Gustafsson M., Persson B., Thyberg J. and Johansson J. (2001) Prediction of amyloid fibril-forming proteins. J. Biol. Chem. **276:** 12945–12950
25 Kuwata K., Li H., Yamada H., Legname G., Prusiner S. B., Akasaka K. et al. (2002) Locally disordered conformer of the hamster prion protein: a crucial intermediate to PrP^{Sc}? Biochemistry **41:** 12277–12283
26 Peretz D., Williamson R. A., Matsunaga Y., Serban H., Pinilla C., Bastidas R. B. et al. (1997) A conformational transition at the N terminus of the prion protein features in formation of the scrapie isoform. J. Mol. Biol. **273:** 614–622
27 Williamson R. A., Peretz D., Pinilla C., Ball H., Bastidas R. B., Rozenshteyn R. et al. (1998) Mapping the prion protein using recombinant antibodies. J. Virol. **72:** 9413–9418
28 Callebaut I., Tasso A., Brasseur R., Burny A., Portetelle D. and Mornon J. P. (1994) Common prevalence of alanine and glycine in mobile reactive centre loops of serpins and viral fusion peptides: do prions possess a fusion peptide? J. Comput. Aided Mol. Des. **8:** 175–191
29 Welker E., Raymond L. D., Scheraga H. A. and Caughey B. (2002) Intramolecular versus intermolecular disulfide bonds in prion proteins. J. Biol. Chem. **277**: 33477–33481
30 Welker E., Wedemeyer W. J. and Scheraga H. A. (2001) A role for intermolecular disulfide bonds in prion diseases? Proc. Natl. Acad. Sci. USA **98:** 4334–4336
31 Prusiner S. B. and Scott M. R. (1997) Genetics of prions. Annu. Rev. Genet. **286:** 593–606
32 Caughey B. (2001) Interactions between prion protein isoforms: the kiss of death? Trends Biochem. Sci. **26:** 235–242
33 Tompa P., Tusnady G. E., Friedrich P. and Simon I. (2002) The role of dimerization in prion replication. Biophys. J. **82:** 1711–1718
34 Serpell L. C., Sunde M. and Blake C. C. F. (1997) The molecular basis of amyloidosis. Cell. Mol. Life Sci. **53:** 871–887
35 Janowski R., Kozak M., Jankowska E., Grzonka Z., Grubb A., Abrahamson M. et al. (2001) Human cystatin C, an amyloidogenic protein, dimerizes through three-dimensional domain swapping. Nat. Struct. Biol. **8:** 316–320
36 Staniforth R. A., Giannini S., Higgins L. D., Conroy M. J., Hounslow A. M., Jerala R. et al. (2001) Three-dimensional domain swapping in the folded and molten globule states of cystatins, an amyloid-forming structural superfamily. EMBO J. **20:** 4774–4781
37 Huang Z., Prusiner S. B. and Cohen F. E. (1995) Scrapie prions: a three-dimensional model of an infectious fragment. Fold Des. **1:** 13–19

38 Warwicker J. (2000) Modeling a prion protein dimer: predictions for fibril formation. Biochem. Biophys. Res. Commun. **278:** 646–652
39 Nicholson E. M., Mo H., Prusiner S. B., Cohen F. E. and Marqusee S. (2002) Differences between the prion protein and its homolog Doppel: a partially structured state with implications for scrapie formation. J. Mol. Biol. **316:** 807–815
40 Blake C. and Serpell L. (1996) Synchrotron X-ray studies suggest that the core of the transthyretin amyloid fibril is a continuous beta-sheet helix. Structure **4:** 989–998
41 Jamin N., Coïc Y.-M., Landon C., Ovtracht L., Baleux F., Neumann J.-M. et al. (2002) Most of the structural elements of the globular domain of murine prion protein form fibrils with predominant β-sheet structure. FEBS Lett. **529:** 256–260
42 Bousset L., Belrhali H., Melki R. and Morera S. (2001) Crystal structures of the yeast prion Ure2p functional region in complex with glutathione and related compounds. Biochemistry **40:** 13564–13573
43 Bousset L., Thomson N. H., Radford S. E. and Melki R. (2002) The yeast prion Ure2p retains its native α-helical conformation upon assembly into protein fibrils in vitro. EMBO J. **21:** 2903–2911
44 Schlumpberger M., Wille H., Baldwin M. A., Butler D. A., Herskowitz I. and Prusiner S. B. (2000) The prion domain of yeast Ure2p induces autocatalytic formation of amyloid fibers by a recombinant fusion protein. Protein Sci. **9:** 440–451
45 Gabus C., Auxilien S., Pechoux C., Dormont D., Swietnicki W., Morillas M. et al. (2001) The prion protein has DNA strand transfer properties similar to retroviral nucleocapsid protein. J. Mol. Biol. **307:** 1011–1021
46 Gabus C., Derrington E., Leblanc P., Chnaiderman J., Dormont D., Swietnicki W. et al. (2001) The prion protein has RNA binding and chaperoning properties characteristic of nucleocapsid protein NCP7 of HIV-1. J. Biol. Chem. **276:** 19301–19309
47 Cordeiro Y., Machado F., Neto L. J., Juliano M. A., Brentani R. R., Foguel D. et al. (2001) DNA converts cellular prion protein into the β-sheet conformation and inhibits prion peptide aggregation. J. Biol. Chem. **276:** 49400–49409
48 Nandi P. K., Leclerc E., Nicole J.-C. and Takahashi M. (2002) DNA-induced partial unfolding of prion protein leads to its polymerisation to amyloid. J. Mol. Biol. **322:** 153–161
49 Salmona M., Malesani P., De Gioia L., Gorla S., Bruschi M., Molinari A. et al. (1999) Molecular determinants of the physicochemical properties of a critical prion protein region comprising residues 106–126. Biochem. J. **342:** 207–214
50 Levy Y., Hanan E., Solomon B. and Becker O. M. (2001) Helix-coil transition of Pr 106–126: molecular dynamic study. Proteins **45:** 382–396
51 Sanghera N. and Pinheiro T. J. T. (2002) Binding of prion protein to lipid membranes and implications for prion conversion. J. Mol. Biol. **315:** 1241–1256
52 Baron G. S., Wehrly K., Dorward D. W., Chesebro B. and Caughey B. (2002) Conversion of raft associated prion protein to the protease-resistant state requires insertion of PrP-res (PrP^{Sc}) into contiguous membrane. EMBO J. **21:** 1031–1040
53 Pillot T., Drouet B., Pincon-Raymond M., Vandekerckhove J., Rosseneu M. and Chambaz J. (2000) A nonfibrillar form of the fusogenic prion protein fragment [118–135] induces apoptotic cell death in rat cortical neurons. J. Neurochem. **75:** 2298–2308
54 Tompa P., Tusnady G. E., Cserko M. and Simon I. (2001) Prion protein: evolution caught en route. Proc. Natl. Acad. Sci. USA **98:** 4431–4436
55 Chen S. G. (1995) Truncated forms of the human prion protein in normal brain and in prion diseases. J. Biol. Chem. **270:** 19173–19180
56 Riek R., Wider G., Billeter M., Hornemann S., Glockshuber R. and Wüthrich K. (1998) Prion protein NMR structure and familial human spongiform encephalopathies. Proc. Natl. Acad. Sci. USA **95:** 11667–11672
57 Zerovnik E. (2002) Amyloid-fibril formation: proposed mechanisms and relevance to conformational disease. Eur. J. Biochem. **269:** 3362–3371
58 Smith C. J., Drake A. F., Banfield B. A., Bloomberg G. B., Palmer M. S., Clarke A. R. et al. (1997) Conformational properties of the prion octa-repeat and hydrophobic sequences. FEBS Lett. **405:** 378–384
59 Merz P. A., Somerville R. A., Wisniewski H. M., Manuelidis L. and Manuelidis E. E. (1983) Scrapie-associated fibrils in Creutzfeldt-Jakob disease. Nature **306:** 474–476
60 Diringer H., Gelderblom H., Hilmert H., Özel M. and Edelbluth C. (1983) Scrapie infectivity, fibrils and low molecular weight protein. Nature **306:** 476–478
61 Merz P. A., Rohwer R. G., Kascsak R., Wisniewski H. M., Somerville R. A., Gibbs C. J. et al. (1984) Infection-specific particle from the unconventional slow virus diseases. Science **225:** 437–440